Voltage Waveform Tailoring for High Aspect Ratio Plasma Etching of SiO_2 using $Ar/CF_4/O_2$ Mixtures: Consequences of Ion and Electron Distributions on Etch Profiles

Florian Krüger[1], Hyunjae Lee[2], Sang Ki Nam[2], and Mark J. Kushner[1,3]

[1] Electrical Engineering and Computer Science Department, University of Michigan, 1301 Beal Ave., Ann Arbor, MI 48109-2122 USA fkrueger@umich.edu, mjkush@umich.edu

[2] Mechatronics R&D Center, Samsung Electronics Co., Ltd., 1-1 Samsungjeonja-ro, Hwaseong-si, Gyeonggi-do 18448, South Korea hj0928.lee@samsung.com, sangki.j.nam@samsung.com

[3] Author to whom correspondence should be addressed.

Abstract:

The quality of high aspect ratio (HAR) features etched into dielectrics for microelectronics fabrication using halogen containing low temperature plasmas strongly depends on the energy and angular distribution of the incident ions (IEAD) onto the wafer, as well as potentially that of the electrons (EEAD). Positive ions, accelerated to high energies by the sheath electric field, have narrow angular spreads and can penetrate deeply into HAR features. Electrons typically arrive at the wafer with nearly thermal energy and isotropic angular distributions and so do not directly penetrate deeply into features. These differences can lead to charging of the insides of the features which can slow etching rates and produce geometric defects such as twisting. In this work, we computationally investigated the plasma etching of HAR features into SiO_2 using tailored voltage waveforms in a geometrically asymmetric capacitively coupled plasma sustained in an $Ar/CF_4/O_2$ mixture at 40 mTorr. The tailored waveform consisted of a sinusoidal wave and its higher harmonics with a fundamental frequency of 1 MHz. We found that some degree of control of the IEADs and EEADs is possible by adjusting the phase of higher harmonics φ through the resulting generation of electrical asymmetry and electric field reversal. However, the IEADs and EEADs cannot easily be separately controlled. The control of IEADs and EEADs are inherently linked. The highest quality feature was obtained with a phase angle $\varphi = 0°$ as this value generated the largest (most negative) DC self-bias and largest electric field reversal for accelerating electrons into the feature. That said, the consequences of voltage waveform tailoring (VWT) on etched features is dominated by the change in the IEADs. Although VWT does produce EEADs with higher energy and narrower angular spread, the effect of these electrons on the feature compared to thermal electrons is not large. This smaller impact of VWT produced EEADs is attributed to thermal electrons being accelerated into the feature by electric fields produced by the positive in-feature charging.

Keywords: Voltage Waveform Tailoring, Plasma Etching, High Aspect Ratio Etching, Electric Field Reversal, Plasma Sheath

I. Introduction

Plasma etching of dielectrics, such as SiO_2, is an integral step in manufacture of micro- and nanometer scale electronics [1-4]. The particular process of etching high aspect ratio (HAR) features is becoming an increasingly critical process due to the complexity of 3-dimensional structures such as 3D-NAND memory. Fabricating these devices require etching HAR contact holes through hundreds of layers of SiO_2 and Si_3N_4 with a total aspect ratio of up to 100 [5-7] with increasing densities of features. These highly anisotropic etches are achieved with energetic ion bombardment with near normal angles of incidence onto the wafer. In capacitively coupled plasmas (CCPs), which are commonly used for plasma etching of dielectrics, the anisotropy of the positive ions is a consequence of acceleration of the ions in the electric field in the sheath bounding the wafer. The majority of HAR etching of dielectrics is performed in CCPs sustained in fluorocarbon gas mixtures, typically using multiple radio frequency (RF) power supplies having frequencies of a few MHz to tens of MHz [7-10] These discharges are usually operated with gas pressures of tens of mTorr with hundreds of watts to many kW of power deposition over a 30 cm diameter wafer. These conditions produce ion fluxes to the wafer of 10^{15}-10^{16} $cm^{-2}s^{-1}$ [11]. Ions (or hot neutrals after ion scattering from the inner sidewalls of features) reaching the bottom of HAR features must have a critically high energy and narrow angular distribution to continue the etch. To achieve these goals, substrate biases having voltages of many kV are regularly used [11-14].

In single frequency electropositive RF discharges, the bulk plasma potential is generally positive with respect to bounding surfaces, leading to an electric field in the sheath above the wafer that points towards the wafer surface during most of the RF cycle [15-16]. This electric field accelerates positive ions into the wafer with high energies and narrow angular spreads, while confining the electrons to the bulk plasma. It is only during a small fraction of the RF cycle at which time the sheath collapses that electron fluxes are able to reach the wafer [17-18]. (By sheath collapse, we refer to the sheath potential rapidly decreasing to small values.) The highly anisotropic, high energy ions can penetrate deeply into HAR features. The electrons incident onto the wafer typically have nearly thermal energy and angularly broad distributions, and so do not naturally penetrate deeply into features [1]. When etching dielectric (or low conductivity materials), these conditions can result in the lower echelons of the feature being charged positively and the upper echelons being charged negatively [19]. This differential charging generates electric field components within the feature [19-21]. The intra-feature electric fields can deviate ion trajectories which

can lead to undesired consequences including mask deformation [22,23], a reduction of the ion flux at the bottom of the feature [24], and profile distortion such as notching, twisting and bowing [19-21]. Negative charging of the mask, a process that is sensensitive to the incident energy distributions of both electrons and ions, may then also produce deviations in the trajectories of incident charged particles [22,23].

The issue of differential charging has previously been addressed by increasing the ion energies to minimize the deflection of ions by intra-feature electric fields. However, this approach must overcome several challenges. The coinciding increase in the power density at the wafer surface can lead to excessive wafer heating which, unchecked, can stress the thermal budget of the process [8,25]. In high volume manufacturing (HVM) this strategy requires the use of technologically complex wafer cooling. Although successful to date, power onto the wafer and wafer cooling has their limits.

Since the desired increase in ion energy is often achieved by increasing the applied voltage to the substrate, another challenge arises in that the sheath thickness is a function of the sheath voltage and by extension the CCP voltage applied to the substrate. Increasing the sheath thickness for otherwise the same process conditions will lead to an increase in the number of collisions in the pre-sheath and sheath, producing a lower energy and broader angular distribution of the incident ion flux. The higher ion energies can also decrease selectivity of the dielectric etch with respect to the mask as the result of an increase in non-selective physical sputtering of the mask. Maintaining high selectivity is critical during the typically long etch times required for HAR features [1,8].

In a typical CCP of the type used for plasma etching in microelectronics fabrication (pressures of tens of mTorr, frequencies of 1 – 100 MHz), the net charged particle flux to surfaces in contact with the plasma must sum to zero over the RF cycle in the steady state,

$$\int_0^T \left(\Gamma_e(t) - \Gamma_i(t)\right) dt = 0 \tag{1}$$

where, T is the RF period. $\Gamma_e(t)$ and $\Gamma_i(t)$ are the time dependent fluxes to the surface of electrons and positive ions, acknowledging that the flux of negative ions is negligible in the absence of pulsing. The electric fields in the sheath and presheath usually point towards surfaces to accelerate ions out of the plasma and to confine electrons. It is only during a small portion of the anodic part of the RF cycle that the sheath voltage decreases sufficiently to allow electrons to reach the

substrate. These electrons arrive at the substrate with largely thermal, isotropic velocity distributions.

Voltage waveform tailoring (VWT) is a technique that is able to provide additional flexibility in producing ion energy and angular distributions (IEADs) onto the wafer [26]. VWT can also be used to generate directional (anisotropic), high energy electron fluxes onto the substrate through promoting an electric field reversal (EFR) in the presheath above the substrate [17]. EFR refers to the electric field in the presheath momentarily pointing into the plasma, as opposed to pointing towards the surface. In VWT, a non-sinusoidal voltage is applied to the substrate, typically using several harmonics of a fundamental frequency. EFR in the presheath ultimately results from the requirement that the time average of positive and negative fluxes to the substrate must balance. Only during the sheath collapse during the anodic part of the cycle are electrons able to diffuse to the surface. Under certain conditions, this diffusive electron transport may not be sufficient to satisfy the local charge balance. These conditiosn include short sheath collapse times, thick sheaths or magnetically or collisionally hindered transport. For these conditions, negative space charge in the presheath produces an EFR, which slows the transport of ions and increases the transport of electrons towards the wafer. Electric field reversal has been observed computationally as well as experimentally [17, 27-30]. In the context of VWT, EFR it was found to be most prevalent when using waveforms that facilitate a rapid and brief sheath collapse [17, 26].

With its ability to produce anisotropic IEADs which naturally penetrate deeply into HAR features, and electron energy and angular distributions (EEADs) onto the substrate which can potentially penetrate deeply into HAR features, VWT has been proposed as a (partial) remedy for neutralizing charging inside HAR features [17,26]. Other techniques can also be used to inject high energy electrons into features. For example, the top electrode of CCPs can be biased with a negative DC voltage, which produces a high energy beam of anisotropic electrons onto the wafer [31]. This technique would require an additional power supply and its associated complexities. The use of tailored waveforms does increase complexity in terms of power supply, harmonic filters and match box designs [32]. The DC generated electron-beam solution requires a counter electrode and so would not be easily implemented into inductively coupled plasma (ICP) systems, whereas the VWT solution is, in principle, applicable to the bias in ICP systems. Ultimately, the choice of the most expedient system will likely be application dependent.

In principle, if the flux of positive ions and negative electrons arriving on the wafer and

reaching the lower echelons of the features can be balanced over the RF cycle, the detrimental effects of intra-feature charging can be avoided. That said, the production of the EFR that accelerates electrons into the wafer and narrows the EEAD requires manipulating the sheath potential during the RF cycle and so the IEADs are also affected. As a result, independent control of the energy and angular distributions (EADs) of both electrons and ions is challenging. From a practical perspective in an actual CCP etching tool, it is not possible to hold the IEAD constant while varying the EEAD using VWT.

The dynamics of VWT, and EFR in particular, are sensitive to the geometry of the plasma reactor and the electronegativity of the plasma. (Electronegativity refers to the ratio of negative ions to electrons. Highly electronegative plasmas have a large ratio of negative ions to electrons, while the RF cycle averaged plasma potential and floating potential are still positive.) For example, one of the features of VWT is the electrical asymmetry effect (EAE) in which the dc bias in a symmetric, multi-frequency CCP can be controlled by the amplitude and phase of the harmonics used in the bias waveform [33,34]. The plasma reactors used in HVM are typically geometrically asymmetric and produce a negative DC bias on the substrate on this basis alone. Using VWT, the DC bias resulting from the EAE then either decreases or increases the geometrically produced DC bias. Electronegative plasmas further complicate the VWT produced EAE and EFR as space charge is maintained by far less mobile negative ions compared to electrons.

In this paper we discuss results from a computational investigation of a multi-frequency CCP sustained in an $Ar/CF_4/O_2$ mixture using a geometry similar to those found in HVM. High frequency power applied to the top electrode is used to sustain the plasma while VWT is used to define the low-frequency bias voltage applied to the bottom electrode. The consequences of the electrical asymmetry effect and the electric field reversal on the IEADs and EEADs onto the wafer surface are discussed. The resulting charged and neutral particle fluxes and distributions are then used in self-consistent simulations of etching a HAR feature into SiO_2 to investigate the ability of VWT to control feature properties.

We found that in spite of the complicating factors of geometry, gas mixture and multiple frequencies, VWT allowed for effective control of IEADs and EEADs onto the wafer, though this control could not be produced independently. Optimizing the waveform to produce a desired EEAD inevitably affects the IEAD. Peak and mean energies of positive ions and of electrons onto the wafer are strong functions of the shape of the applied voltage waveform. With the narrow

angle and energetic EEADs produced by VWT, our investigation did show a decrease in intra-feature charging, as measured by a decrease in the positive electrical potential. However, the overall characteristics of the final etch feature was dominated by the ion dynamics.

Synthetic changes to only the EEADs resulted in minor changes of the final etched feature. For example, there were not significant differences in feature quality between an isotropic, thermal EEAD onto the wafer corresponding to an electron temperature of a 3-4 eV, and the narrow, energetic EEAD produced by VWT. We attribute this result to the fact that thermal electrons are accelerated into the feature by the electric fields produced by the positive, in-feature electric potential. Ultimately, in a quasi-steady state, the flux of positive and negative charge into the feature must be equal. This is achieved by producing a positive potential in the feature, which then accelerates thermal electrons into the feature. The narrow energetic EEADs produced by VWT are also accelerated into the feature. However, their initially higher wafer directed velocities require a smaller positive potential in the feature to achieve the needed flux balance. The end result is a decrease in the intra-feature potential relative to that produced with thermal electrons that is approximately equal to the average energy of the VWT produced EEAD.

The computational platform used for the reactor scale plasma transport, the Hybrid Plasma Equipment Model (HPEM) and the reactor conditions are discussed in Sec. II. The Monte Carlo Feature Profile Model (MCFPM) used for the feature scale simulations of etching, and its application here, are described in Sec. III. The influence of phase angle φ of the voltage waveform on charged particle distributions onto the wafer and etch profiles with low bias power is discussed in Sec. IV and with high bias power is discussed in Sec. V. Concluding remarks are in Sec. VI.

II. Description of the Reactor Scale Model

The investigation of the reactor scale plasma dynamics was performed using the Hybrid Plasma Equipment Model (HPEM), which is described in detail in Ref. [35]. In short, the HPEM is a 2-dimensional hydrodynamic model which resolves plasma phenomena in a time-slicing approach. Different physics regimes are addressed in modules that are coupled by exchanging physical quantities – electric and magnetic fields, densities, rate coefficients. The major modules used in this work are the Fluid Kinetics-Poisson Module (FKPM), the Electron Energy Transport Module (EETM), and the Plasma Chemistry Monte Carlo Module (PCMCM).

In the FKPM, the continuity, momentum, and energy equations of the heavy particles are

solved coincidently with Poisson's equation to provide heavy particle densities, fluxes and electrostatic potential. Electron densities and fluxes in the bulk plasma are addressed using continnum, fluid techniques in the FKPM. In the EETM, the spatially dependent electron energy distributions (EEDs) in the plasma are obtained using a kinetic, Monte Carlo based approach using the space and phase resolved electric fields produced in the FKPM [36]. These EEDs are then used to produce electron impact rate coefficients and transport coefficients for use in the FKPM. The trajetories of secondary electrons produced by ion impact and excited state impact on surfaces are addressed using fully kinetic, Monte Carlo techniques in the EETM. The energy and angular distribution of electrons striking the substrate are recorded in the EETM, which are then used as input to the MCFPM. The EEDs for both bulk and secondary electrons are continuously updated during the simulation by repeatedly executing the EETM.

After the plasma reaches a quasi-steady state the PCMCM, using Monte Carlo techniques, tracks the trajectories of ions and reactive neutral species. EADs of these species are recorded impinging onto the wafer and are used as input to the MCFPM. The reaction mechanism used for $Ar/O_2/CF_4$ plasmas is described by Vasenkov et al [37,38]. That reaction mechanism has been modified by updating the model for Ar excited states to include the processes described in [39]. Ion induced secondary electron emission coefficients on surfaces in contact wtih the plasmas was included using coefficients of 0.15 and 0.05 for wafer and metals. Excited Ar species induce secondary electron emission with a probability of 0.01 on all surfaces [40].

A schematic of the cylindrically symmetric CCP reactor used in this investigation is shown in Fig 1. The reactor, modeled after multi-frequency CCPs used in industrial HVM applications, consists of two parallel plate electrodes with a diameter of 300 mm separated by a 2.8 cm gap. A silicon wafer is mounted on the bottom electrode and a showerhead gas inlet is distributed across the top electrode. A focus ring made of silicon and quartz to improve discharge uniformity surrounds the wafer. The dielectric constants of these components are $\varepsilon/\varepsilon_0 = 4$ for the outer quartz ring and $\varepsilon/\varepsilon_0 = 11.8$ for the Si ring. While the conductivity of the quartz is negligible, that of the Si wafer is 0.05/Ω-cm. The feedstock gas $Ar/CF_4/O_2$ = 75,/15/10 flows at 500 sccm through the top electrode. The reactor pressure is held constant at 40 mTorr at the location of the pressure sensor near the pump port by throttling the rate of pumping.

The VWT power supply is connected to the bottom electrode through a blocking capacitor of 500 nF. In principle, in the quasi-steady state, the DC bias should be independent of the value

of the blocking capacitor provided that the RC time constant of the plasma-capacitor series impedance is large compared to transients in current. The capacitance used here is a balance of there being an acceptably short charging time and long enough RC time constant so that there is little variation in the DC bias during the RF cycle.

Sheath properties are in part a function of plasma density at the edge of the sheath which then determines sheath thickness. To maintain a relatively constant plasma density and to minimize sheath variation based on changes in plasma density, 500 W is coupled into the plasma through the top electrode using a sinusoidal voltage waveform with a frequency of 80 MHz. This power was maintained by continually adjusting the amplitude of the voltage at 80 MHz.

To control the dynamics of charged particles impinging on the wafer surface, a customized voltage waveform, $V(t)$, was applied to the bottom electrode. The waveform consists of a fundamental sine wave with a frequency f_0 = 1 MHz and 4 consecutive higher harmonics,

$$V(t) = V_0 \sum_{i=1}^{N} \frac{N-k+1}{N(N+k)} \cos(2k\pi f_0 t + k\pi\varphi_k) . \quad (2)$$

Here, V_0 is the total applied voltage amplitude, k is the harmonic order, N is the total number of frequencies, and the relative phase shift of each harmonic frequency k is φ_k. In this work the number of harmonics is N = 5. The consequences of VWT were investigated by varying the phase shift of the even harmonics φ for k = 2, 4. The resulting waveforms are shown in Fig. 2 for phase shifts of φ = 0°, 45°, 90°, 135° and 180°. The power coupled through the bottom electrode, P_0, was initially held constant at 1 kW by adjusting V_0.

III. Description of the Feature Scale Model

The EADs sampled at the substrate surface were used as input to the Monte Carlo Feature Profile Model (MCFPM) to simulate the evolution of etch features in semiconductor device materials [40,41,42]. Briefly, MCFPM is a voxel based, kinetic model in which pseudo-particles representing gas phase species are launched with energies and angles sampled from the EADs obtained from the HPEM. The trajectories of the incoming particles are integrated, with charged particles subject to acceleration by electric fields, until a collision with a surface occurs. The specific surface reaction is chosen based on a stochastic Monte Carlo approach. Depending on the reaction, the voxel representing the surface site is removed (physical or chemical sputtering), chemically modified (passivation) or a voxel is added on top of the site (deposition). Species

reflected from or produced at the surface, such as a sputter or chemical etch product, are returned to the gas phase, and their trajectories are tracked until they are consumed in a reaction at a surface or leave the feature. Although the capability exists in the MCFPM to have electron stimulated surface chemistry or electron implantation, in this study, electrons do not modify the surface other than through depositing their charge.

In this study, we investigated the plasma etching of SiO_2 in a $Ar/O_2/CF_4$ gas mixture. A detailed description of the reaction mechanism is given by Huang et al. [40]. Generally, all incoming ions or hot neutrals resulting from neutralization of ions when striking surfaces can physically sputter every material according to the incident particles mass, angle and energy as well as the surface binding energy of the material. Radical C_xF_y species can lead to the deposition of polymer, the main contributor to sidewall passivation, which in turn is removed by sputtering and etching by oxygen radicals. C_xF_y radicals can react with the SiO_2 surface to create a layer of $SiO_2C_xF_y$ complexes, significantly lowering the binding energy and making the complex easier to chemically sputter.

The electric potential in the feature was computed by collecting charge on surfaces and solving Poisson's equation. The relative permittivity for SiO_2 used in solution of Poisson's equation was $\varepsilon_r = 4.0$, and for photoresist, polymer and $SiO_2C_xF_y$ complexes was $\varepsilon_r = 3.0$. The electric potential then provides electric fields used to advance the trajectories of charged particles. All positive ions neutralized when striking a surface, and if reflected, continued as a neutral. Electrons were collected on surfaces with unity probability. For this study, the SiO_2 and photoresist had essentially zero conductivity ($10^{-10}/\Omega$-cm). Polymer ($5\times10^{-6}/\Omega$-cm) and $SiO_2C_xF_y$ complexes ($1\times10^{-6}/\Omega$-cm) had finite but small conductivity. These conditions generally resulted in charge being resident only on surfaces, or buried under polymer or redeposited etch products if deposition occurred on top of charged surfaces.

The geometry used for the feature evolution is shown in Fig. 3. The feature is a trench consisting of a 3000 nm thick SiO_2 layer over a Si stop-layer, covered by 100 nm thick photoresist with a 100 nm opening. This geometry produces an aspect ratio of about 30 for an etched trench down to the stop layer. The simulation was performed in 3-dimensions as a finite depth trench. The mesh consists of 60 cells wide by 750 cells tall by 10 cells deep, producing cubic voxels with 5 nm edge length. Reflective boundary conditions are used along the y-axis normal to the geometry shown in Fig. 2. Although we are simulating a nominally 2-dimensional feature (a trench),

performing the simulation in 3-dimensions results in a more realistic representation of sidewall roughness. When simulating a trench in 2-dimensions, sidewall roughness is effectively uniform (and infinite) in the unresolved depth. In 3-dimensions, sidewall roughness is finite. The etching was performed for a fixed time of 15 minutes.

The Monte-Carlo method which is used in the MCFPM inherently produces statistical variation in the details of the features that are produced. This run-to-tun variation can occur naturally in parallel computations by differences in the timings of the processors. The statistical variation features can be demonstrated by changing the seeds for the random number generators on separate runs. The features shown here are typical, average features in which outliers due to statistical variation have been excluded. The statistical run-to-run differences in features are discussed in Appendix A.

IV. Plasma and Etch Properties for 1000 W of VWT Power

In industrial applications of plasma etching, it is most common to control power deposition in the plasma as opposed to voltage amplitude. To make more direct connection to these applications, the power applied through the VWT on the bottom electrode was first held constant at P_{VWT} = 1000 W by adjusting the voltage amplitude V_0 while varying the phase φ from 0 – 180°. Although this power appears large, by industrial processing standards for HAR etching of 30 cm diameter wafers, 1000 W is a moderately small power [40,43,44]. The applied voltage amplitudes necessary to maintain constant power coupling through the top electrode (500 W), bottom electrode (P_{VWT} = 1000 W) and the resulting DC self-bias on the bottom electrode are shown in Fig. 4 as a function of phase angle. At constant power, the amplitude of the high frequency voltage applied to the top electrode is a weak function of the phase angle and is nearly constant at V_{HF} = 120 V. The DC self-bias, however, is strongly coupled to φ with its magnitude decreasing (becoming more positive) by 88% from V_{dc}= -2480 at φ=0° to V_{dc}= -290 at φ=0°.

Earlier works have described the trend of how DC bias depends of the shape of the applied waveform through the generation of the electrical asymmetry effect (EAE) [18,45]. The DC self-bias can be expressed as

$$V_{dc} = -\frac{V_{\max} + \beta V_{\min}}{1+\beta}, \tag{2}$$

where $V_{\max}$ and $V_{\min}$ are the maximum and minimum of the applied voltage. β is the discharge

symmetry parameter given by

$$\beta = \left(\frac{A_p}{A_g} \right)^2 \frac{\overline{n}_{sp}}{\overline{n}_{sg}} \frac{I_{sg}}{I_{sp}}, \tag{2}$$

where the areas of the powered and ground electrodes are A_p and A_g and the ion densities near the powered and grounded surfaces are $\overline{n}_{sp}$ and $\overline{n}_{sg}$. I_{sp} and I_{sg} are the sheath integrals, described in prior publications on the origin of the EAE [33, 34, 45]. In short, these are dimensionless quantities that depend only on the normalized profile of the sheath charge density.

The formulation for the EAE does not specifically account for a second powered electrode having a unique frequency, such as used here. However, due to the higher frequency and lower power of this second RF bias, the voltage amplitude applied to the top electrode is smaller than that applied to the lower electrode. Sinusoidal voltages alone do not induce electrical asymmetry effects and so we do not expect large perturbations to the EAE process by the high frequency source. With the phase shift applying only to the tailored waveform on the bottom electrode, V_{HF} remains relatively constant for all φ, varying by less than 10%. Due to the changes to the electron dynamics in the sheath region some variation does occur in V_0, decreasing from 2800 V to 2200 V or about 27% from $\varphi = 0$ to 180°.

The DC self-bias on the lower electrode, V_{DC}, is an important parameter in determining the energy of incident positive ions. For high frequency excitation where the energy width of the IEAD is small compared to the RF voltage amplitude, the centroid in energy of the IEAD typically increases with the magnitude of V_{DC}. With low fundamental frequencies (thin sheath limit), ions transiting the sheath respond to the sheath dynamics during the RF period. (This is nearly always true for electrons.) In this low frequency limit, the correlation between IEAD and V_{DC} is not straight forward.

The radially averaged axial electric field as a function of time and distance from the substrate, $E_z(z, t)$, is shown in Fig. 5 for phase shifts of $\varphi = 0°$ to 180°. In CCPs without an electric field reversal, $E_z(z, t)$ near the bottom electrode sheath will point towards the electrode (negative z direction) at all times. However, with $\varphi = 0°$, an EFR occurs during the sheath collapse at around 0.5 μs when the applied voltage is at its maximum positive value and there is a positive electric field component (pointing in +z direction). This EFR results, in part, from the short duration of the positive voltage excursion of the voltage waveform and the correspondingly short time during

which the sheath collapses. In order to produce the required electron flux to the surface to maintain a charge-neutral flux to the substrate, an EFR occurs to accelerate electrons towards the surface. This field reversal is most pronounced in the $\varphi = 0°$ case (69 V/cm) as this phase has the shortest sheath collapse and so requires the largest instantaneous electron flux to the surface. As the duration of the sheath collapse increases with increasing φ and becomes less abrupt, the magnitude of the instantaneous electron flux that is required to balance charge decreases, and so the magnitude of the EFR reversal also decreases.

The modulation of the sheath as a function of the phase of the harmonics translates into significant variation of IEADs incident onto the wafer, as shown in Fig 6a. These IEADs are collected by summing over all ions striking the wafer for $\varphi = 0°$ to 180°. The IEADs generally decrease in maximum energy with increasing φ, following the trend in V_{dc}. The mean energy of the ions also decreases with increasing φ, as shown in Fig 6c. Aside from the general decrease in energy, the shape of the IEADs reflect the temporal dynamics of the sheath. The IEAD for $\varphi = 0°$ contains a dominant peak at 3000 eV, a result of the sheath maintaining a nearly constant potential and thickness for the majority of the RF cycle. (See Fig. 5.) The IEADs for $\varphi = 45°$, 90° and 135° contain more complex multi-modal structures with broader spreads in energy. The structure in the IEADs reflects the length of time the sheath is maintained at a given potential and thickness. The IEAD for $\varphi = 180°$ has a single dominant peak at approximately 400 eV, as the sheath has one of two quasi-binary states – fully collapsed or fully expanded.

The EEADs incident onto the wafer surface are shown in Fig. 6b for $\varphi = 0°$ to 180°. The electric field reversal for small values of φ produces a significant acceleration of electrons normal to the surface, generating an EEAD with a higher energy and narrower angular distribution that might occur with low frequency, sinusoidal waveforms. (Recall that for a purely thermal distribution of electrons onto the surface, the mean energy will be about the electron temperature, 3-4 eV, and the angular spread would span -90° to +90°.) The EEAD for $\varphi = 0°$, where the EFR has is largest magnitude, extends to 125 eV, considerably higher than the thermal bulk temperature of about 3.2 eV. (Although the electron energy distribution is non-Maxwellian in the bulk plasma, for convenience we will refer to the electron flux incident onto the electrode in the absence of significant EFR as being the thermal electron flux or resulting from thermal electrons.) The downward trend of the magnitude of the electric field reversal with increasing φ in turn leads to a decrease in the electron acceleration normal to the surface, and so to an overall reduction in electron

energy incident onto the surface. With φ = 180°, the EEADs incident onto the surface closely resemble a thermal distribution, though with a somewhat narrower angular distribution. The high energy, low angle electrons are likely the result of electrons accelerated in the sheath at the opposing elelctrode. Due to the 2 decade log scale of the image, these structures are visually overemphasized.

In addition to the charged particle EADs onto the surface, the silicon-dioxide etching mechanism depends on the magnitude of the individual fluxes of charged and neutral species onto the wafer. In particular, the ratio of polymer depositing and polymer removing species is important in dielectric etching in fluorocarbon containing plasmas. The time averaged fluxes of neutral and ion species onto the wafer as a function φ are shown in Fig. 7. With changes in φ there are systematic changes in EADs of charged particles onto the surface. However, the neutral fluxes are fairly stable with moderate variation with changes in phase φ for most species. With the high frequency power being held constant, the rates of electron impact dissociation and ionization are nearly constant, producing nearly constant fluxes. The small variation in neutral fluxes with φ can be attributed to the contribution to dissociation by secondary electrons emitted from the wafer and accelerated by the sheath into the bulk plasma. With the electron energy distribution of the secondary electrons being functions of sheath dynamics, rates of dissociation will also vary.

Similar trends apply for the fluxes of ions to the wafer as a function of φ, which also show little variation with phase both in terms of overall magnitude as well as the relative ratios of ion fluxes. The one notable exception is the flux of O^+ which increases for intermediate values of φ. The atomic weight of O^+ is the lightest of ions having a significant flux to the surface and so will respond more quickly to changes in the sheath (and presheath) compared to other ions. There is also likely a component of ionization of atomic oxygen by high energy secondary electrons. Given that the fluxes of Ar^+ and CF_3^+ are 2 orders of magnitude higher than that of O^+, we do not expect this sensitivity of the flux of O^+ on phase angle to have a large effect on etch properties.

The feature profiles for trenches in SiO_2 after 15 min of plasma etching are shown in Fig. 8a for phase angles of φ = 0° to 180°. Varying φ for constant power produces significant differences in etch depth, ranging from 1750 nm for φ = 0° to an immediate etch stop due to excessive polymer buildup at φ = 180°. Due to the similar absolute fluxes of reactants for all phase angles, this trend in etch depth is a consequence of the differences in charged particle energy distributions onto the wafer resulting from the change in applied voltage waveforms. The higher energy of the

incident ions at low phase angles produces higher rates of removal of passivating polymer films and higher rates of sputtering of SiO_2, directly or by chemically assisted processes. The etch stop at $\varphi = 180°$ is a consequence of the lower ion energies that are unable to balance the deposition of polymer by removal of polymer by sputtering. A net etch at $\varphi = 180°$ would be possible for lower rates of polymer deposition (lower incident fluxes of CF_x radicals).

The higher incident energies of the positive ions also enable them to partially overcome positive electrical potential that builds up inside features. This positive potential slows ions, thereby reducing their sputter yield with possible deflection of their trajectories inside the features, which leads to twisting. One of the original motivations for VWT was to promote in-feature charge neutralization on surfaces by narrowing the angular distribution of electrons to better match that of the ions. These narrow and energetic EEADs presumably would penetrate deeper into the feature than is possible by the broad, low energy thermal EEADs produced by conventional CCPs. The desired end result would be a charge neutral feature.

To test this hypothesis, one would need to perform reactor scale simulations where the ion and neutral fluxes, and IEADs remain the same, while the EEADs varied from low energy, broad angle to high energy, narrow angle. From our attempts to find such conditions, we conclude that the likelihood is small of being able to hold the IEAD constant while varying the EEAD. The very conditions that modify the EEADs also modify the IEADs. A large set of computational experiments were performed to find combinations of voltage, power and waveforms that would maintain the same IEAD while toggling between a nearly thermal EEAD, and an EFR enhanced EEAD. We were not able to find such conditions.

Instead, to test the hypothesis that EEADs produced by electric field reversals can decrease the magnitude of positive charge in the feature the following process was used. Etch profiles were compared when using EEADs produced from using VWT and a synthetic thermal EEAD having a 3 eV electron temperature. The fluxes of radicals and ions, and IEADs, were the same for both cases. These reference simulations were performed for $\varphi = 0°$. For these conditions, the differences in EEADs between those generated by VWT and synthetic thermal distributions are the greatest. The VWT case, $\varphi = 0°$ also resulted in the overall most desirable feature profile.

The etch profiles and corresponding final electric potential are shown in Fig. 8b for the (left) self consistently generated VWT produced EEAD and (right) for the synthetic thermal EEAD. Both cases have both negative and positive charge distributed throughout the feature,

though with net negative charge at the top of the features and net positive charge deeper in the feature. The end result is positive potential inside the feature. The maximum potential with the VWT produced EEAD is 227 V and the maximum potential produced with the thermal electrons is 346 V. The larger positive potential with thermal electrons reduces the final etch depth by 30% by slowing the positive ions incident into the feature. This result confirms the initial hypothesis that directional electrons produced by the EFR can be utilized to at least partially neutralize intra-feature surface charging and lessen the decrease in etch rate resulting from that charging.

The maximum ion energy incident into the feature exceeds 3000 eV. If there was no electron neutralization of positive charge in the feature, the positive potential would increase to nearly this maximum value to prevent positive charge from being continually collected. Even when using the thermal electron EEAD, the potential inside the feature is significantly smaller than the maximum ion energy. The thermal electrons initially have isotropic trajectories which dominantly strike the top of the feature. However, the buildup of positive potential in the feature produces electric fields directed upwards that then accelerate these thermal electrons into the feature. The thermal electrons accelerated into the feature then produce significant neutralization of positive charge on the sidewalls.

In the steady state, the positive potential inside the feature increases to a large enough magnitude so that the thermal electrons accelerated into the feature are able to neutralize incremental additions to positive charge. This transient is directly analogous to the charging of a dielectric surface in contact with a plasma to a negative potential that balances the flux of electrons and ions. The use of the VWT produced EEAD, with its initially higher energy and velocities towards the wafer, and narrower angular distribution, enables this balance of electron and ion fluxes to be achieved with a lower positive potential. The difference in electric maximum potential in the features between the thermal EEAD and the VWT produced EEAD, 120 V, corresponds to approximately the difference in the maximum energy of the VWT produced and thermal EEADs. Although this is not a general result, the difference in potential would not be expected to exceed this value.

When using the VWT generated and thermal EEADs, the location of maximum potential is not at the bottom of the feature but at depths of 1.2 μm for the VWT EEAD and 0.77 μm for the thermal EEAD. The charging of the mask is nominal compared to the energies of ions and EFR accelerated electrons. The mask charging may be more important for low aspect ratio (AR)

features where the voltages and powers are lower. However, for HAR features, this is typically not an issue. The maximum of the positive potential is a function of AR. As the feature is etched deeper and the AR increases, the maximum in positive potential transitions from the bottom of the feature at low AR to the side of the feature as the AR increases [40]. For small AR, ions even with a finite angular spread can directly strike the bottom of the feature, and so the maximum positive potential is on the bottom of the feature. For HAR features, ions having a finite angular spread will strike the sidewalls, and positive charging will occur dominantly on the sidewalls. The neutralized particles then proceed as hot neutrals deeper into the feature. The shadowing by the fairly thick photoresist produces a view angle of 3.8° (VWT) to 4.3° (thermal) which is in line with the ion angular spreads.

The charging of the feature occurs over many RF cycles. There are no specific in-feature, intra-cycle dynamics of the electric field as the charging and electric fields are the results of averaging charged particle fluxes over these many RF cycles. For bias frequencies of many MHz and above, distinct cyclic in-feature electric field dynamics will likely only occur when using pulsed power.

Electron trajectories inside the feature depend on their initial distribution in energy and angle as well as the acceleration resulting from electric fields in the feature produced by charge deposition. In the case with the highest electron energy incident onto the wafer ($\varphi = 0°$) the mean energy of the EEAD is 62 eV. Given the maximum electric potential in the feature is 280 V, the electron trajectories are still likely dominated by the electric fields produced by charging. To verify this likelihood, electron energies incident onto the surface inside the feature were spatially sampled. To enable a side-by-side comparison of these energies, the following process was followed. The feature shape and potential configuration resulting from the $\varphi = 0°$ case after 15 minutes of etching was used and kept constant. (That is, no further evolution of the feature or potential was allowed.) Initial electron trajectories were sampled from the EEAD produced by VWT or from a thermal distribution having an electron temperature of 3 eV. The electron trajectories were followed into the feature, and the electron energies striking the surface were recorded and averaged at each spatial location. Tests were performed for VWT produced EEAD and thermal distributions when including acceleration from the charge produced electrics fields, and when excluding that acceleration.

The resulting spatially resolved average electron energies incident on the feature surface

are shown in Fig. 9. The average energies shown in Fig. 9a are for initial EEADs (VWT and thermal) when including acceleration in the electric fields produced by charging. The average energies striking the surface for VWT and thermal distributions are spatially similar, and qualitatively resemble the electric potential shown in Fig. 8b. These distributions largely result from acceleration of the incident electrons by the in-feature electric fields. The average energy of the electrons striking the surface for the initially thermal electrons is maximum at about 240 eV, which corresponds to the maximum positive potential inside the feature. The average energy for the electrons launched from the VWT produced EEAD is maximum at about 275 eV. This value is larger than for the thermal electrons by 35-40 eV due to the electrons selected from the VWT produced EEAD beginning their trajectories with significant initial velocities.

To reinforce this finding, average electron energies striking the surface of the feature were computed for the VWT produced EEAD and for thermal electrons when excluding acceleration by electric fields, as shown in Fig. 9b. The average energies for the VWT produced EEAD range up to 35 eV and those for the thermal EEAD range up to 6 eV, both values largely reflecting the initial distributions.

These findings suggest that for reasonably large positive potentials produced inside features, the high energy VWT produced EEADs will not dominate the resulting feature properties compared to EEADs produced using conventional waveforms. In both cases, in the steady state electrons are accelerated into the feature in such a manner as to neutralize the incremental charge produced by fluxes of positive ions. This is particularly true for positive potentials that are much larger than the average energy of the incident EEADs.

V. Plasma and Etch Properties for 2000 W of VWT Power

While maintaining 500 W of power on the top electrode, the power delivered by the bottom electrode was increased to P_{VWT} = 2000 W to be more aligned with industrial processes. The resulting voltage amplitudes for the top and bottom electrodes, and the DC self-bias are shown in Fig. 4b as a function of phase angle. The top electrode voltage amplitude remains nearly unchanged compared to the P_{VWT} = 1000 W cases with there being little variation with phase angle φ. In order to accommodate the increase in power, the bottom electrode voltage amplitude increased by a factor of 1.5-2 compared to the P_{VWT} = 1000 W cases. The low- and high-power cases have nearly identical trends with phase angle, which suggests that these trends are the result

of the sheath dynamics rather than being of stochastic origin. Similar to the 1000 W cases, V_{dc} decreases with increasing phase angle as a consequence of the EAE. The large magnitude of V_{dc} correlates to the larger applied voltage amplitude.

The radially averaged, axial electric fields as a function of time during the RF cycle for P_{VWT} = 2000 W are shown in Fig. 10 for different phase angles φ. Overall, the sheath dynamics and electric field reversals as a function of phase angle are similar to the P_{VWT} = 1000 W cases (Fig. 5) with the EFR decreasing with phase. One exception is the $\varphi = 0°$ case whose EFR is reduced compared to $\varphi = 45°$ at same power and also reduced compared to the $\varphi = 0°$ case at 1000 W. This apparent outlier is the result of the geometrical constraints of the plasma reactor and of the finite electrode gap (distance between bottom and top electrodes). For example, the spatially resolved electron densities averaged over the RF period are shown in Fig. 11 for $\varphi = 0°$, 90° and 180°. While the peak electron densities vary by only about 10% the spatial distributions vary considerably with change in φ.

With low values of φ, the time averaged sheath thickness is larger, which reflects the larger (more negative) DC bias and voltage amplitude. The sheath thickness then occupies a significant fraction of the gap. The compressed bulk plasma is then more sensitive to, for example, discontinuities between the top electrode and the bounding dielectric insulator where electric field enhancements occurs. The end result is a less spatially uniform plasma. We acknowledge that, if unaddressed, this expansion of the sheath could potentially affect the spatial uniformity of the wafer processing, and that this effect may be amplified by this particular reactor configuration. Several reactor configurations were investigated (e.g., adjusting the shape and diameter of the focus rings, and top electrode) to confirm that the VWT scaling discussed here, and sheath expansion and plasma compression are general trends. There are many actions, such as adjusting the process parameters (gas composition, gas pressure, flow rates, power) and/or reactor geometry that could be used to recoup the trends with phase angle that were obtained at the lower power. This optimization, is beyond the scope of this work. That said, this demonstration emphasizes the concept that design of plasma processing reactors must be performed from a systems perspective. Optimizing one aspect of the design, such as EFR, may ultimately be limited by other aspects of the design, such as gap dimension.

The similarities to the trends of the lower power cases are also reflected in the IEADs to the wafer as a function of phase angle, are shown in Fig. 12a. While compared to the lower power

cases, the ion energies are higher overall due to the larger voltage amplitudes, the peak energies still decline with increase in the phase angle from a maximum of about 4500 eV for $\varphi = 0°$ to 3000 eV at $\varphi = 180°$. Comparing the cases with highest and lowest ion energies ($\varphi = 0°$ and $\varphi = 180°$), the peak ion energy was reduced by approximately 85% at 1000 W and reduced by 38% for 2000 W. This degree of ion energy control should enable some degree of customizing fluxes for energy-sensitive surface processes. In particular, the distribution of high-energy ions compared to low energy ions within the IEAD is sensitive to phase angle.

These trends for the IEADs are in contrast to the much lighter and more agile electrons, whose EEADs to the wafer are shown in Fig. 12b. The EEADs display the same general trends as in the low power case. The EEADs have high energies and narrow angular spreads for low values of φ compared to thermal distributions due to the electric field reversal produced by VWT. The energies decrease and angular spread increases with increasing phase angle φ. The $\varphi = 0°$ case is, again, a notable exception, having a lower peak energy than a larger phase angle. This exception correlates with the smaller EFR described above. The suppressed electric field reversal due to geometric confinement of the sheath leads to reduced electron acceleration, resulting is the comparatively lower electron energy.

The IEADs, EEADs and fluxes for different phase angles for 2000 W bias power were used as input to otherwise identical MCFPM simulations. The final etch profiles are shown in Fig. 13a. Significant etch depths were reached for all phases, in deference to the $P_{VWT} = 1000$ W cases where an etch stop occurred due to excessive fluxes of polymer forming radicals, or lack of polymer sputtering ions, at large phase angle. There are, however, significant differences in etch depth and overall feature quality. The $\varphi = 0°$ case produces the deepest overall etch while having perhaps a tolerable amount of bowing. The $\varphi = 45°$ case has less bowing but lower etch rate. These trends result from $\varphi = 0°$ case having the higher ion energies (faster overall etch rate) while the $\varphi = 45°$ has a narrower ion angular distribution (less bowing), albeit at a lower energy. Some component of the narrower feature could be a result of the EEAD at $\varphi = 45°$ being more energetic which enables some non-negligible decrease in in-feature charging. The shape of the EEAD is important to moderately increasing etch rate and moderately modifying sidewall slope through neutralizing charge. However, the final feature quality is dominated by the EAD of ions rather than the electrons.

Analogous to the low power case, MCFPM simulations using synthetic thermal EEADs

were performed, and the resulting profiles are compared to etch profiles resulting from VWT produced EEADs in Fig. 13b for $\varphi = 0°$, 90° and 180°. In the $\varphi = 0°$ and 180° cases the differences between the profiles obtained with thermal and VWT EEADs are small and below the statistical threshold discussed in Appendix A. The profile obtained with the VWT EEAD for $\varphi = 90°$ is deeper with a similar amount of tapering compared to the thermal EEAD. These trends result from the EEADs onto the wafer for these conditions having the highest energy and lowest angular spread for intermediate values of φ. This correlation between the improvement of the final etched feature and the energy and directionality of the electrons reinforces the conclusion that these directional electrons enhance the natural neutralization of charge that is produced by acceleration of thermal electrons into the feature. However, the properties of the EEADs do not dominate the shape of the feature.

VI. Concluding Remarks

To investigate the consequences of voltage waveform tailoring (VWT) on etching of SiO_2 using a capacitively coupled $Ar/CF_4/O_2$ plasma, computational investigations of the reactor scale and feature scale processes were performed. While applying 500 W at 80 MHz to the top electrode with the goal of sustaining a constant plasma density, the bottom electrode was driven using VWT composed of consecutive harmonics with a fundamental frequency of 1 MHz at powers of 1000 W and 2000 W. The phase of the even harmonics φ was varied in order to generate electrical asymmetry as well as electric field reversal in the bottom sheath. It was found that changing φ enables control of charged particle dynamics incident onto the wafer surface which in turn translates to significant changes in etch profiles. At low phase angle the EAE as well as the EFR are most significant, which leads to increased energy and directionality of ions as well as electrons onto the wafer.

These favorable distributions in energy and angle increase etch rate by partially reducing the negative effects of intra-feature charging. The directional electrons are better able to reach the lower echelons of the feature and partially neutralize positive charges. The higher energy ions have larger rates of chemical sputtering while also being more able overcome the remaining deflecting electric fields produced by in-feature charging. Overall, for otherwise equal processing conditions and time, low φ cases produced higher etch rates and more favorable sidewall slope. For low bias power, the reduction in ion energy with large values of phase angle resulted in an

etch stop due to the large incident flux of polymerizing radicals. At low bias power, having higher ion energies, sputtering of the polymer enabled competitive etching even at high phase angle.

A key finding of this investigation is the VWT produced EEADs having large energy and narrow angle do not produce the expected significant reductions of in-feature charging compared to thermal EEADs. The VWT produced EEADs did produce somewhat higher etch rates and lower in-feature potentials. However, the buildup of positive charge in the feature accelerates thermal electrons into the feature to energies commensurate with that of the positive potential. The VWT produced EEADs are also accelerated into the feature by this positive potential. If the positive potential is significantly larger than the average energy of the VWT produced EEAD, there is little difference in feature properties between having thermal or VWT generated EEADs. Both are accelerated into the feature by the positive charge to sufficient energy to neutralize, in the steady state, the incremental positive charge brought into the feature by ions.

Another key finding is the need for a systems perspective in process design and in employing VWT in particular. The results of this study showed that at low power, the VWT generated EEADs produced a beneficial effect, enabling higher etch rates for a given power compared to conventional sinusoidal excitation. Conversely, the same etch rate could be sustained at a lower power. We also found that this benefit was not universal. At higher powers, we found that the gap dimension (distance between wafer and top electrode) ultimately limited the ability of VWT to generate electric field reversal and energetic fluxes to the wafer. Low phase angle produces a larger (more negative) DC bias, which thickens the sheath. For a narrow gap CCP, the sheath may consume a large fraction of the gap, which then interferes with the formation of EFR. The fundamental physics of VWT generated EEADs applies to a wide range of powers. However, as with many excitation schemes in plasma etching, the benefits of VWT are likely process dependent, being sensitive to geometry, frequency, pressure and gas mixture.

In the ideal, one would like to tailor an IEAD to best produce the desired etch feature, and then tune the feature profile by tailoring the EEAD. Unfortunately, independently producing specified IEAD and EEAD with the same waveform is difficult. Changing the waveform to generate, for example, the desired EEAD will also affect the IEAD. There may be opportunity to separately tailor the IEAD and EEAD by using binary-pulsed system. The system would consisted of two separate waveforms alternately applied, with one waveform optimized to produce the desired IEAD and the second to produce the desired EEAD.

Acknowledgements

This work was supported by Samsung Electronics Ltd. These results were also based upon work supported by the U.S. Department of Energy, Office of Science, Office of Fusion Energy Sciences under award number DE-SC0020232, and supported by the National Science Foundation (PHY-2009219).

Conflict of Interest

The authors have no conflicts of interest to disclose.

Data Availability

The data that support the findings of this study are available from the corresponding author upon reasonable request.

Appendix A: Statistical Variation in Predicted Feature Profiles

The Monte-Carlo method employed in the MCFPM produces profiles that are inherently subject to statistical variations. This is especially the case when charging processes are included which can act as a feedback loop which amplifies statistical variations. These variations result from the sequence of random numbers that are used to initially generate particle trajectories towards the surface. Quantitiatively different features are produced by changing the *seed* that is used to initialize the random number generators. Even when keeping the same seeds, when executing the simulation in a parallel computing environment, there are nearly unavoidable differences in sequencing of the particle trajectories tracked on different processors. Different random number generators are used for each parallel thread to minimize these sequencing issues, but they will occur.

To ensure the overall validity of results produced when statistical variations occur, it is imperative to verify that the random run-to-run variations are of significantly smaller magnitude than the effects discussed. This includes the overall trends in feature properties as a function of phase angle φ as well as the isolated effects produced by surface charge neutralization by the incident electron flux, perhaps most sensitive to these statistical variations.

To assess the statistical variations, a series of identical simulations was performed while varying the random number seed. These cases also include the inherent statistical variations that occur in the parallel comuting environment. The resulting profiles for the $\varphi = 0°$, $P_{VWT} = 1000$ W

series are shown in Fig. 14a for 15 minutes of etching. The maximum difference from the mean etch depth for this series is less than 5% of the total etch. This variation is less than the change in etch depth and profile shape produced by the change in IEADs as a function of φ observed in this work. Similar conclusions extend to variation between the profiles produced with VWT produced and thermal EEADs.

Statistical variations of this type are not limited to numerical simulations but also occur in actual etch processes, producing a certain degree of feature-to-feature non-uniformity. This statistical feature-to-feature variation results from the small size of features, which in turn produces statistically different fluxes of reactant species into the feature. A common approach to remedy these unwanted statistical variations in HVM processes is *over-etching*. In over-etching, a terminal or etch stop layer is located at the desired final etch depth. For any given process, the etch rate into this layer is significantly lower than for the overlying substrate. This means that once the stop layer is reached during the process, vertical etching effectively stops (or is significnatly slowed) while etching of the tapered side walls continues. Extending the etch process beyond this contact time, over-etching, partially remedies some of the statistical variations in feature profile by straightening the sidewalls of the feature.

A series of profiles are shown in Fig. 14b produced with different random number seeds, analogous to Fig 14a, while etching to the stop layer and over-etching for a total of 30 minutes. Through this over-etching, the variations in etch depth and profile are reduced. Where applicable, etch stop layers and over-etching can suppress the statistical run to run differences in feature properties.

[1] V. M. Donnelly and A. Kornblit, J. Vac. Sci. Technol. A **31,** 050825 (2013).

[2] J. H. Kim, et al., Thin Solid Films **637,** 43 (2017).

[3] K. J. Kanarik, S. Tan and R. A. Gottscho, J. Phys. Chem. Lett. 9, 4814 (2018).

[4] G. S. Oehrlein and S. Hamaguchi, Plasma Sources Sci. Technol. **27**, 023001 (2018).

[5] H. Tanaka, M. Kido, K. Yahashi, M. Oomura, et al., Dig. Tech. Pap. - Symp. VLSI Technol. 14–5 (2007).

[6] S. N. Hsiao, et al., Appl. Surf. Sci. **541,** 148439 (2021).

[7] K. Ishikawa, et al., Jpn. J. Appl. Phys. **57**, 06JA01 (2018).

[8] B. Wu, A. Kumar and S. Pamarthy J. Appl. Phys. **108**, 51101 (2010).

[9] T. Iwase, et al., Jpn. J. Appl. Phys. **58**, SE0802 (2019).

[10] M. Omura, et al., Jpn. J. Appl. Phys. **58**, SEEB02 (2019).

[11] E. G. Shustin, J. Commun. Technol. Electron. **62**, 454 (2017).

[12] H. W. Tak et al., Appl. Surf. Sci. **600**, 154050 (2022).

[13] B. R. Rogers and T. S. Cale, Vacuum **65**, 267 (2002).

[14] I. Adamovich, et al J. Phys. D. Appl. Phys. **50**, 323001 (2017).

[15] R. Sahu, A. Tropina and R. Miles, Phys. Plasmas **29,** 040701 (2022).

[16] M. Klich, et al., Plasma Sources Sci. Technol. **31,** 045014 (2022).

[17] P. Hartmann, et al., J. Phys. D. Appl. Phys. **54,** 255202 (2021).

[18] J. Schulze, et al., J. Phys. D. Appl. Phys. **41**, 105214 (2008).

[19] B. Radjenović and M. Radmilović-Radjenović, Engineering **6**, 1 (2014).

[20] B. M. Radjenović, M. D. Radmilović-Radjenović and Z. L. Petrović IEEE Trans. Plasma Sci. **36**, 874 (2008).

[21] G. S. Hwang, J. Vac. Sci. Technol. B. **15**, 70 (1997).

[22] P. Zhang, L. Zhang and K. Lv, Plasma Chem. Plasma Process. **40,** 1605 (2020).

[23] P. Zhang, L. Zhang and L. Xu, Plasma Process. Polym. **17**, e2000014 (2020).

[24] H. Jansen, et al., Microelectron. Eng. **35**, 45 (1997).

[25] C. Han, et al., Semicond. Sci. Technol. **35**, 045003 (2020).

[26] F. Krüger, S. Wilczek, T. Mussenbrock and J. Schulze, Plasma Sources Sci. Technol. **28,** 75017 (2019).

[27] S. Brandt, et al., Plasma Sources Sci. Technol. **28**, 095021 (2019).

[28] U. Czarnetzki, D. Luggenhölscher and H. F. Döbele, Plasma Sources Sci. Technol. **8**, 230 (1999).

[29] Y. X. Liu, et al., Appl. Phys. Lett. **101**, 114101 (2012).

[30] S. Sharma and M. M. Turner, J. Phys. D. Appl. Phys. **47** 285201 (2014).

[31] M. Wang and M. J. Kushner, J. Appl. Phys. **107,** 023309 (2010).

[32] J. Wang, S. Dine, J.-P. Booth and E. V. Johnson J. Vac. Sci. Technol. A **37,** 021303 (2019).

[33] B. G. Heil, U. Czarnetzki, R. P. Brinkmann and T. Mussenbrock, J. Phys. D. Appl. Phys.

41, 165202 (2008).

[34] J. Schulze, E. Schüngel and U. Czarnetzki, J. Phys. D. Appl. Phys. **42**, 092005 (2009).

[35] M. J. Kushner, J. Phys. D. Appl. Phys. **42,** 194013 (2009).

[36] S. H. Song and M. J. Kushner, Plasma Sources Sci. Technol. **21**, 055028 (2012).

[37] A. V. Vasenkov, X. Li, G. S. Oehrlein and M. J. Kushner, J. Vac. Sci. Technol. A. **22**, 511 (2004).

[38] A. V. Vasenkov and M. J. Kushner, J. Appl. Phys. **95**, 834 (2004).

[39] P. Tian and M. J. Kushner, Plasma Sources Sci. Technol. **24**, 034017 (2015).

[40] S. Huang, et al, J. Vac. Sci. Technol. A **37**, 031304 (2019).

[41] Y. Zhang, et al., J. Vac. Sci. Technol. A Vacuum, Surfaces, Film. **35**, 021303 (2016).

[42] C. M. Huard, S. Sriraman, A. Paterson and M. J. Kushner J. Vac. Sci. Technol. A Vacuum, Surfaces, Film. **36**, 06B101 (2018).

[43] J. K. Kim, et al., J. Vac. Sci. Technol. A **31**, 061302 (2013).

[44] J. K. Kim, S. H. Lee, S. Il Cho and G. Y. Yeom, J. Vac. Sci. Technol. A **33**, 021303 (2014).

[45] U. Czarnetzki, J. Schulze, E. Schüngel and Z. Donkó, Plasma Sources Sci. Technol. **20,** 024010 (2011).

Figures Captions

1. Schematics of the reactor. a) The two frequency CCP has the VWT power applied to the lower electrode and a sinusoidal, 80 MHz waveform applied to the top. b) Electrical schematic of the system. From F. Kruger et al, Plasma Sources Sci. Technol. **30**, 085002 (2021). Reproduced by permission of IOP Publishing Ltd.

2. Voltage waveforms resulting from different phase angles, $\varphi = 0°$ (top) to $\varphi = 180°$ (bottom). The time scale is in units of the period of the fundamental frequency.

3. Initial geometry used in for feature profile simulations. A 700 nm mask defines a 100 nm opening to 3000 nm thick SiO_2. The simulations are for trench etching, performed in 3-dimensions having a finite depth.

4. Voltage amplitudes for the VWT bias (V_{bias}) and top power (V_{top}), and DC self-bias as a function of phase angle. a) $P_{VWT} = 1000$ W and b) $P_{VWT} = 2000$ W.

5. Vertical electric field component as a function of time and distance from wafer for $P_{VWT} = 1000$ W for phase angles of a) 0°, b) 45°, c) 90°, d) 135° and e) 180°. The shape of the voltage waveform applied to the bottom electrode is shown in each image.

6. Properties of ions and electrons incident onto the wafer for $P_{VWT} = 1000$ W. a) IEAD and b) EEAD for phase angles of $\varphi = 0°$, 45°, 90°, 135° and 180°. The distributions are separately normalized and plotted on a log-scale over 2 decades. c) Mean ion energy as a function of phase angle φ.

7. Fluxes of reactive species onto the wafer as a function of phase angle φ. a) Neutrals and b) ions.

8. Feature properties for $P_{VWT} = 1000$ W following 15 minutes of etching a) Feature profiles for different phase angles ($\varphi = 0°$, 45°, 90°, 135° and 180°). b) Comparison of etch result and electric potential for (left) self-consistent VWT produced EEAD and (right) synthetic thermal EEAD. The potentials are separately normalized with the maximum values indicated at the top of the images.

9. Spatial distribution of average electron energies incident on the surface of the feature. The feature properties are for $P_{VWT} = 1000$ W and $\varphi = 0°$ after 15 minutes of etching. Results are shown for initial EEADs produced with VWT and for thermal electrons having a temperature

of 3 eV. a) When including acceleration in electric fields produced by feature charging. b) Without acceleration due to feature charging. The view is looking obliquely into the 3-dimensional feature having reflective boundary conditions front-and-back.

10. Vertical electric field component as a function of time and distance from wafer for P_{VWT} = 2000 W for phase angles of a) 0°, b) 45°, c) 90°, d) 135° and e) 180°. The shape of the voltage waveform applied to the bottom electrode is shown in each image.

11. Electron density for P_{VWT} = 2000 W for phase angle φ of a) 0°, b) 90° and c) 180°). The densities are plotted on a log-scale over 2-decades.

12. Energy and angular distributions for charged particles incident onto the wafer for P_{VWT} = 2000 W for phase angles of φ = 0°, 45°, 90°, 135° and 180°. a) Ions and b) electrons. The distributions are separately normalized and plotted on a log-scale over 2 decades.

13. Feature properties for P_{VWT} = 2000 W following 15 minutes of etching a) Feature profiles for different phase angles (φ = 0°, 45°, 90°, 135° and 180°). b) Comparison of profiles obtained with VWT generated EEADs and synthetic thermal electron distributions for phase angles φ of 0°, 90° and 180°.

14. Statistical run-to-run variation of the final etch profiles for the P_{VWT} = 1000 W and φ = 0° case. a) 15 min run and b) 30 min to produce over etch into the stop layer. For each series of profiles, each case had a different seed for the random number generators, in addition to having the inherent statistical variations in the parallel computing environment.

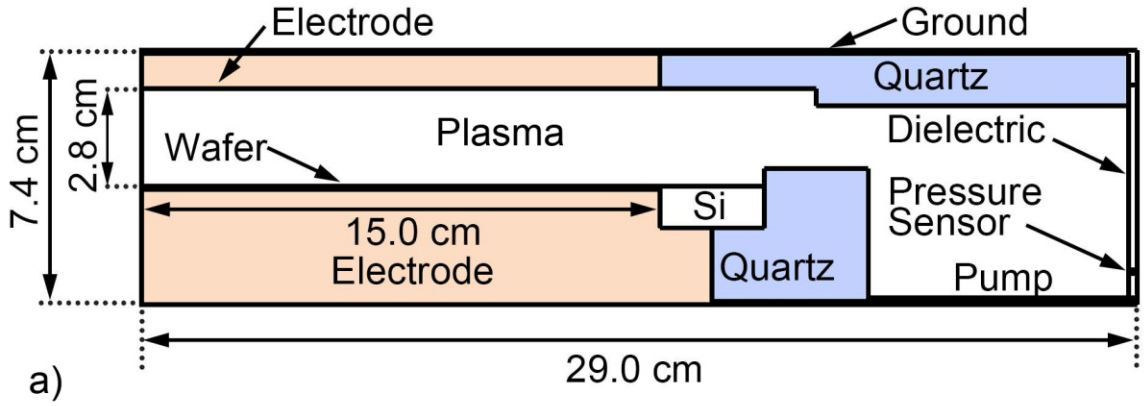

a)

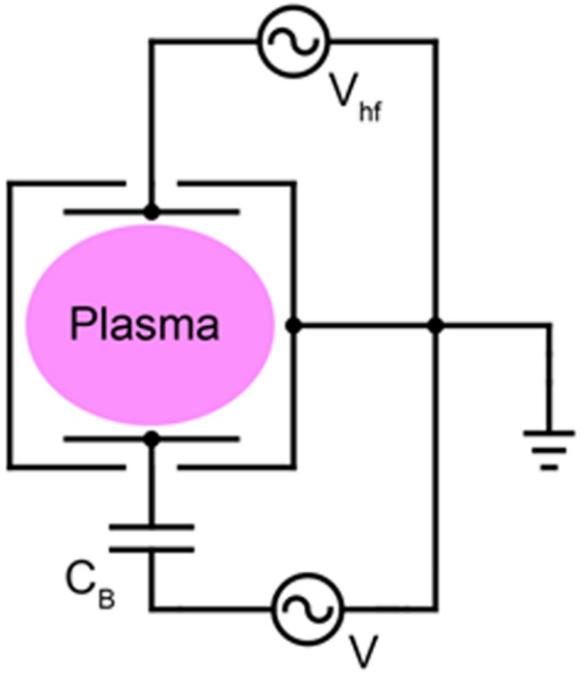

b)

Kruger et al,
Fig. 1 of 14

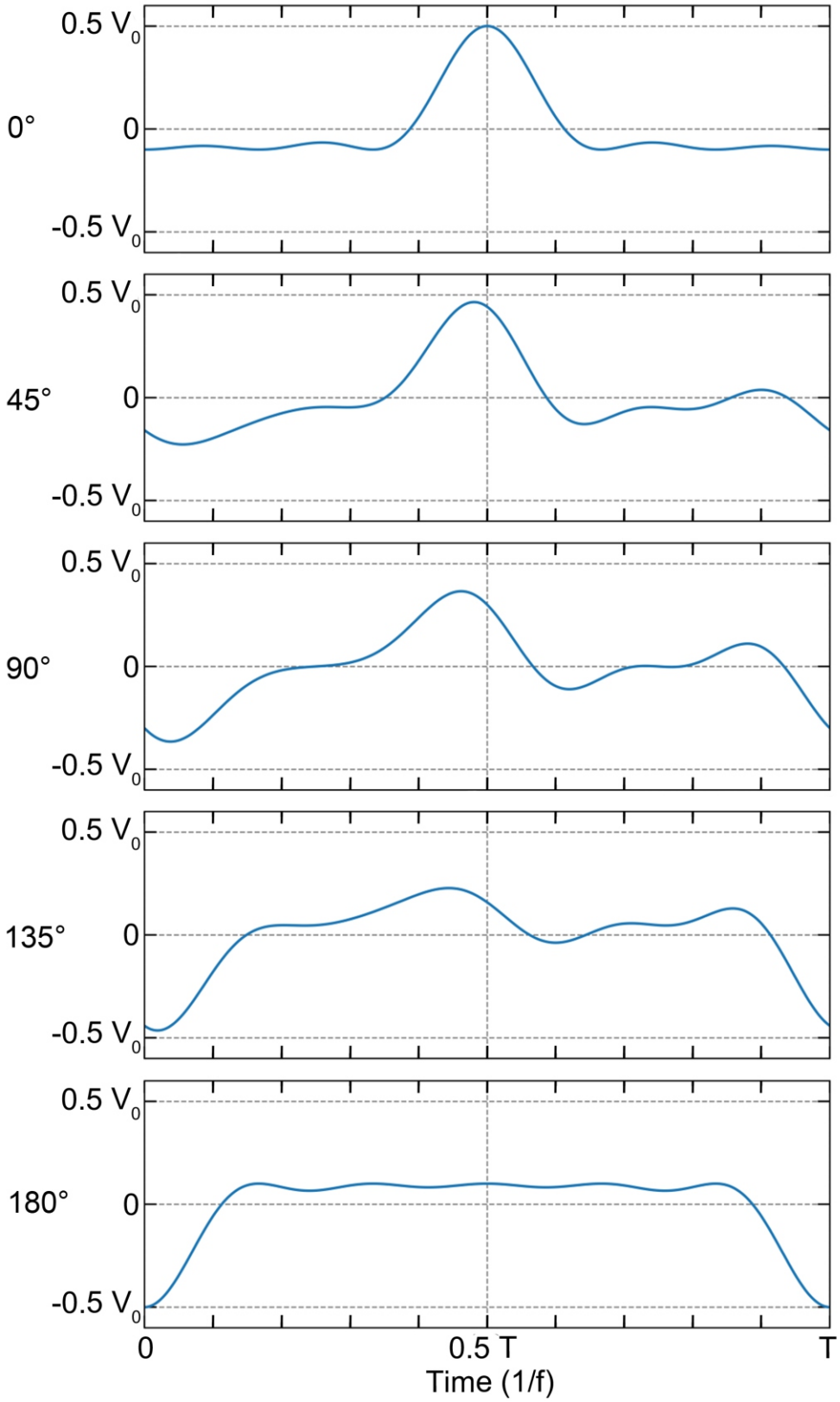

Kruger et al,
Fig. 2 of 14

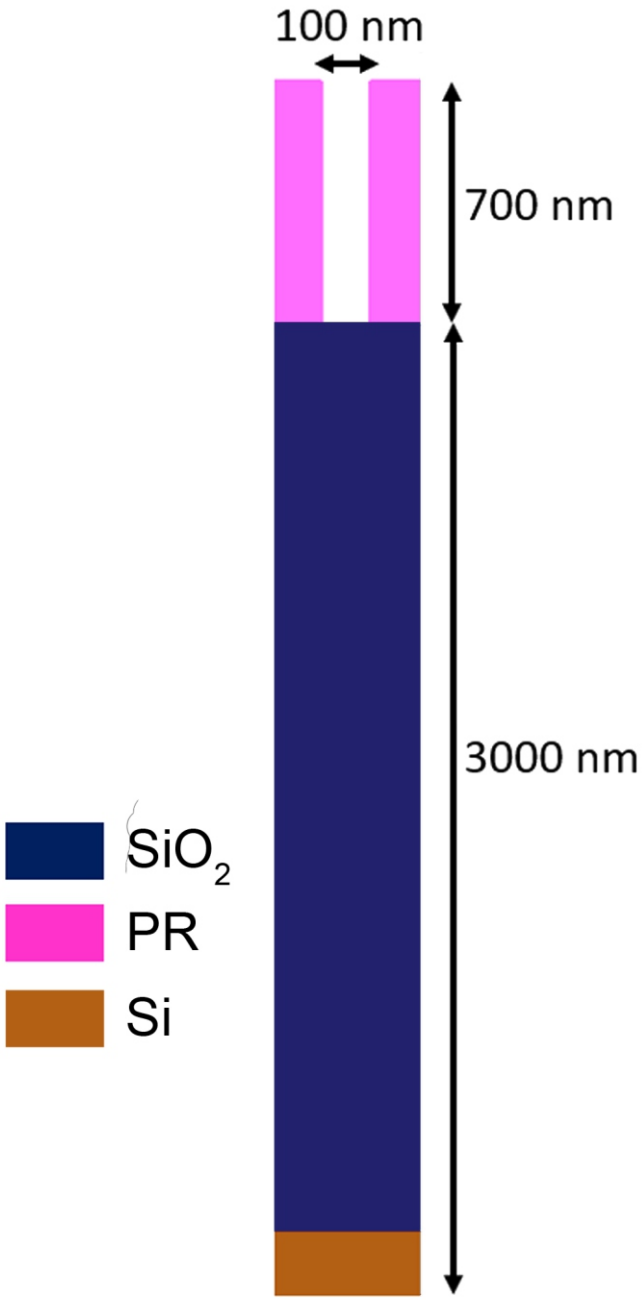

Kruger et al,
Fig. 3 of 14

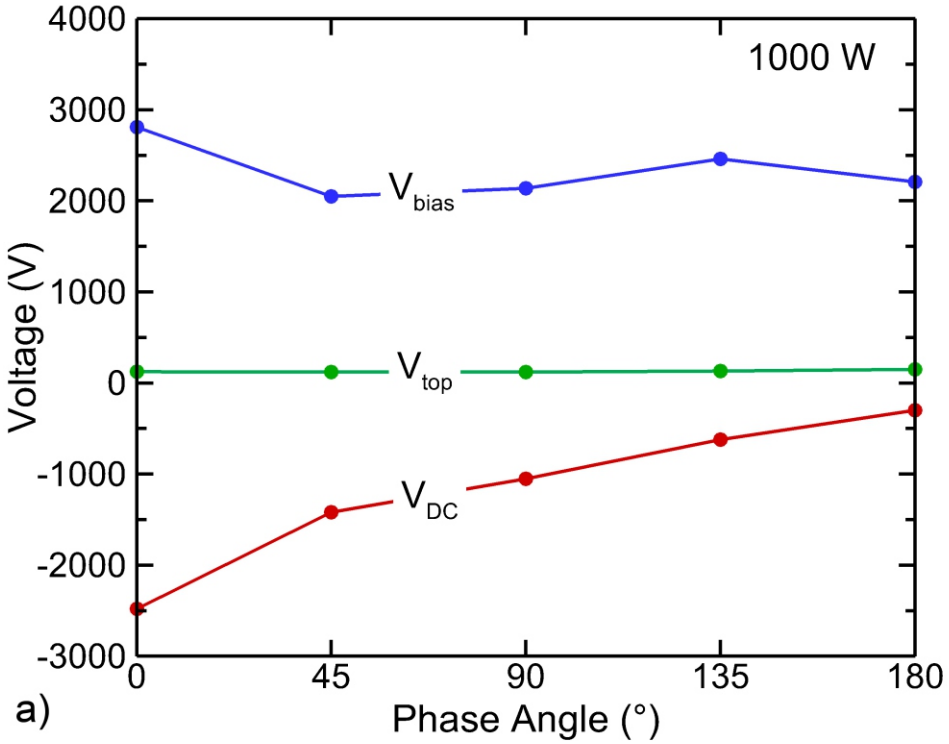

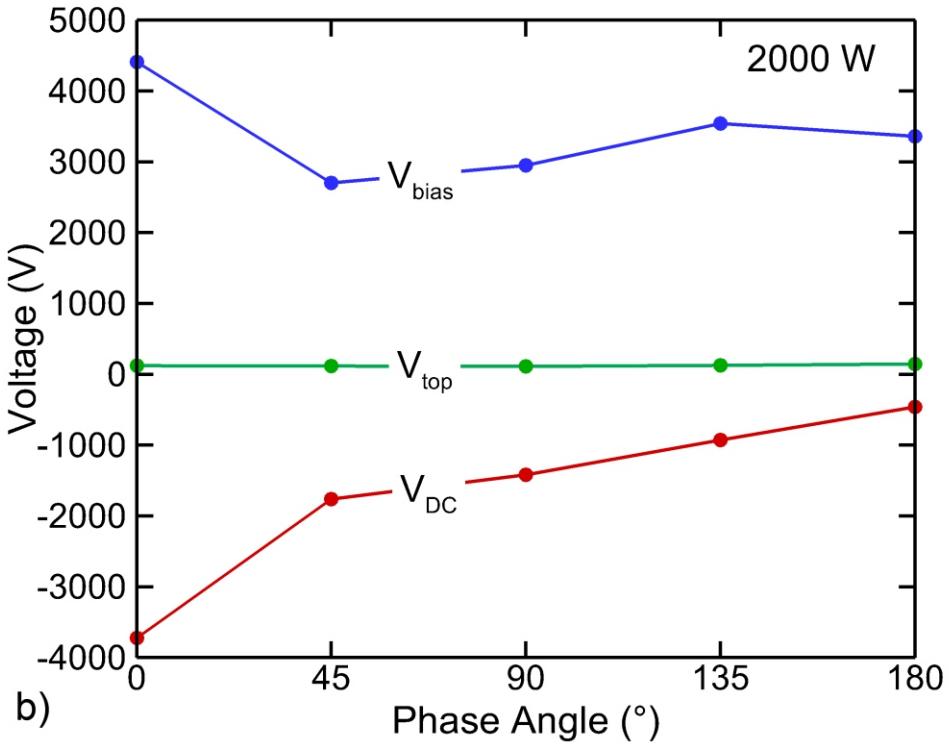

Kruger et al,
Fig. 4 of 14

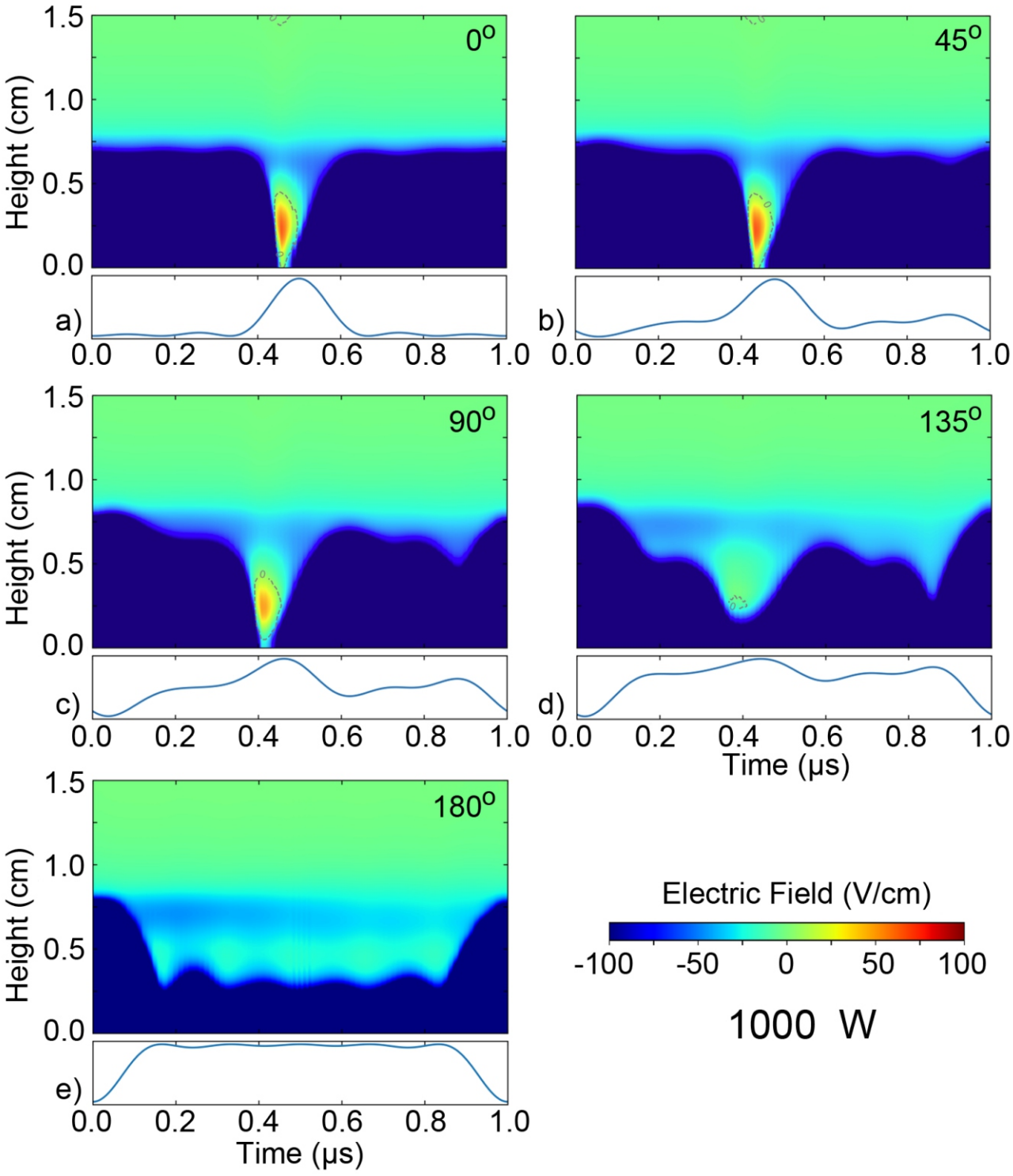

Kruger et al,
Fig. 5 of 14

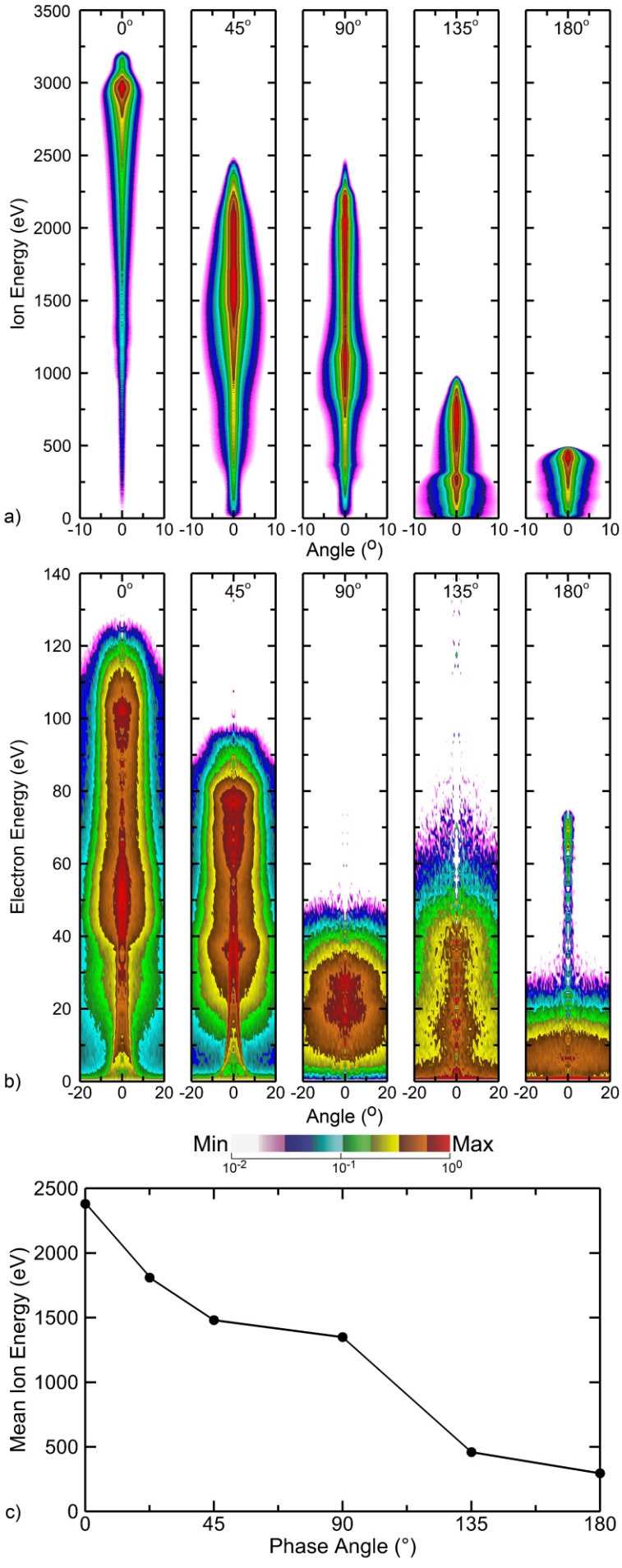

Kruger et al,
Fig. 6 of 14

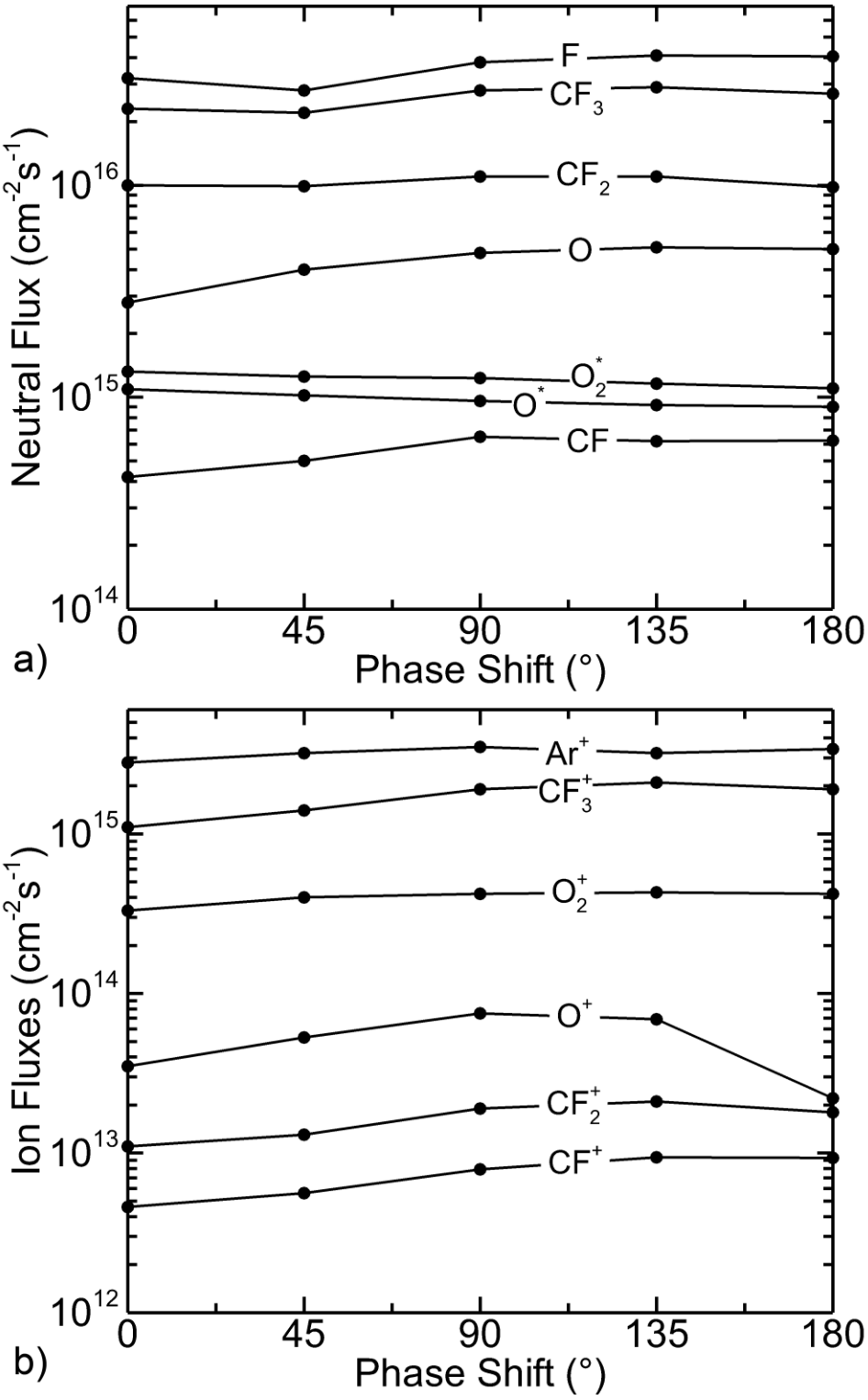

Kruger et al,
Fig. 7 of 14

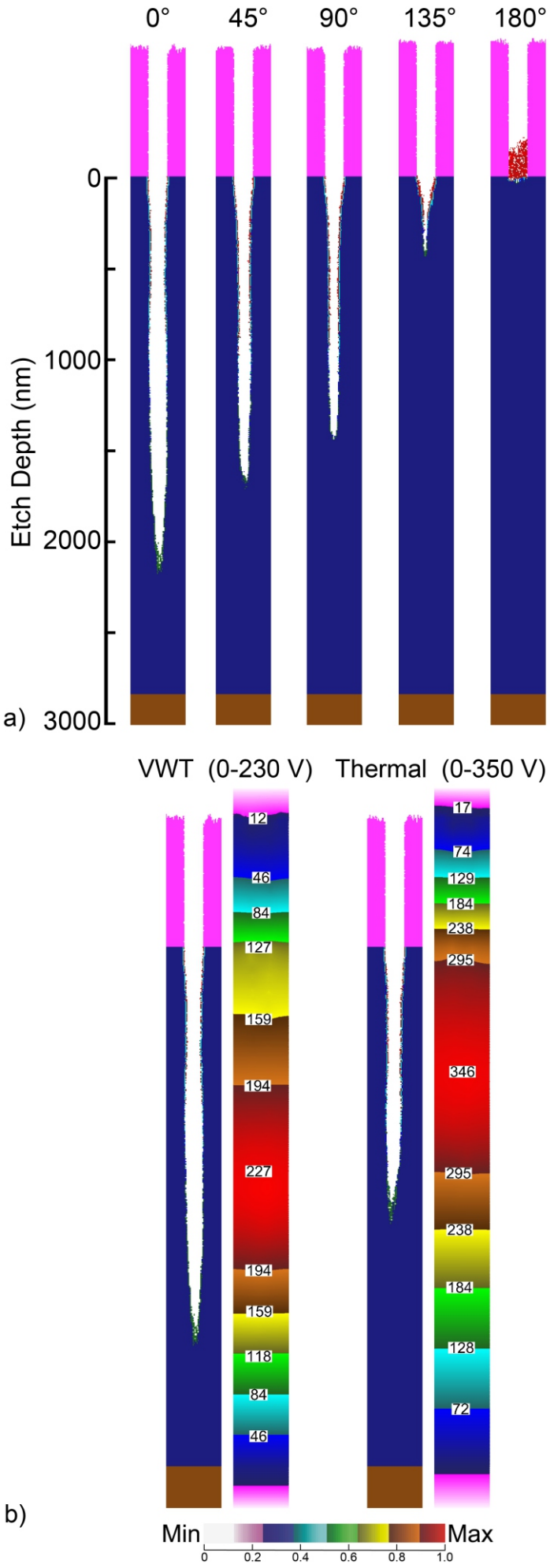

Kruger et al,
Fig. 8 of 14

Kruger et al,
Fig. 9 of 14

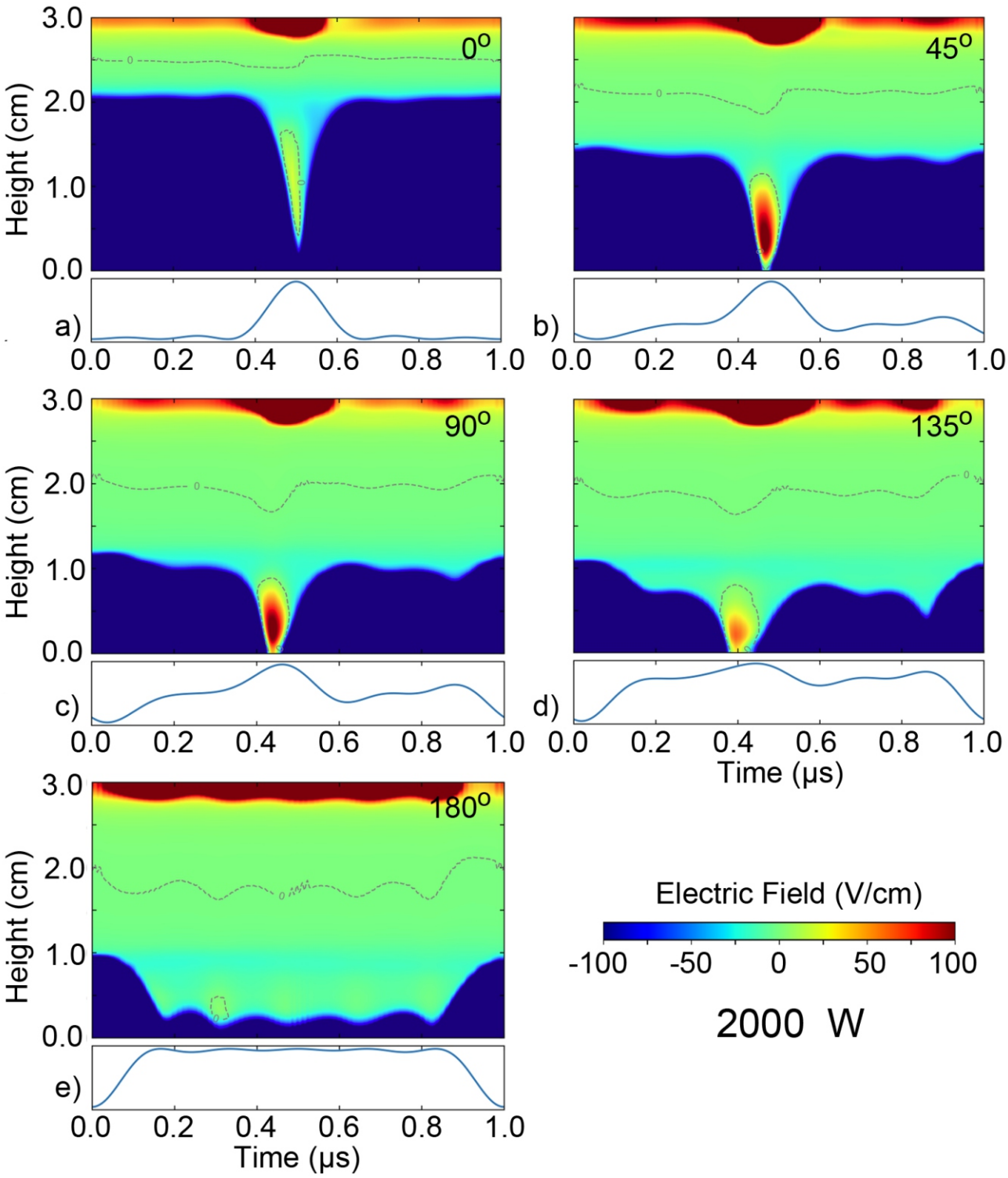

Kruger et al,
Fig. 10 of 14

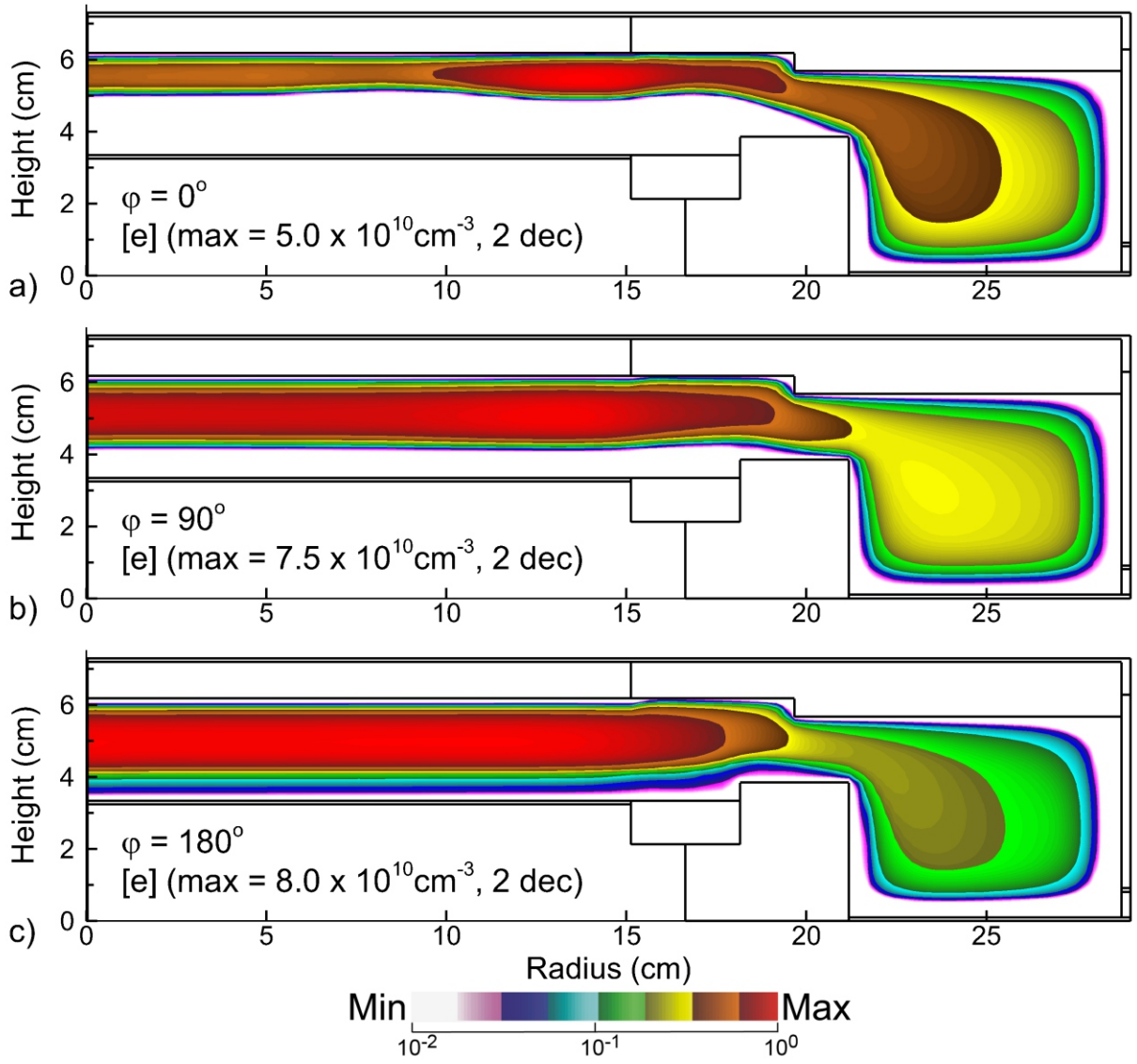
Height (cm)
a)
φ = 0°
[e] (max = 5.0 x 10^10 cm^-3, 2 dec)
b)
φ = 90°
[e] (max = 7.5 x 10^10 cm^-3, 2 dec)
c)
φ = 180°
[e] (max = 8.0 x 10^10 cm^-3, 2 dec)
0
2
4
6
0
5
10
15
20
25
Radius (cm)
Min
Max
10^-2
10^-1
10^0

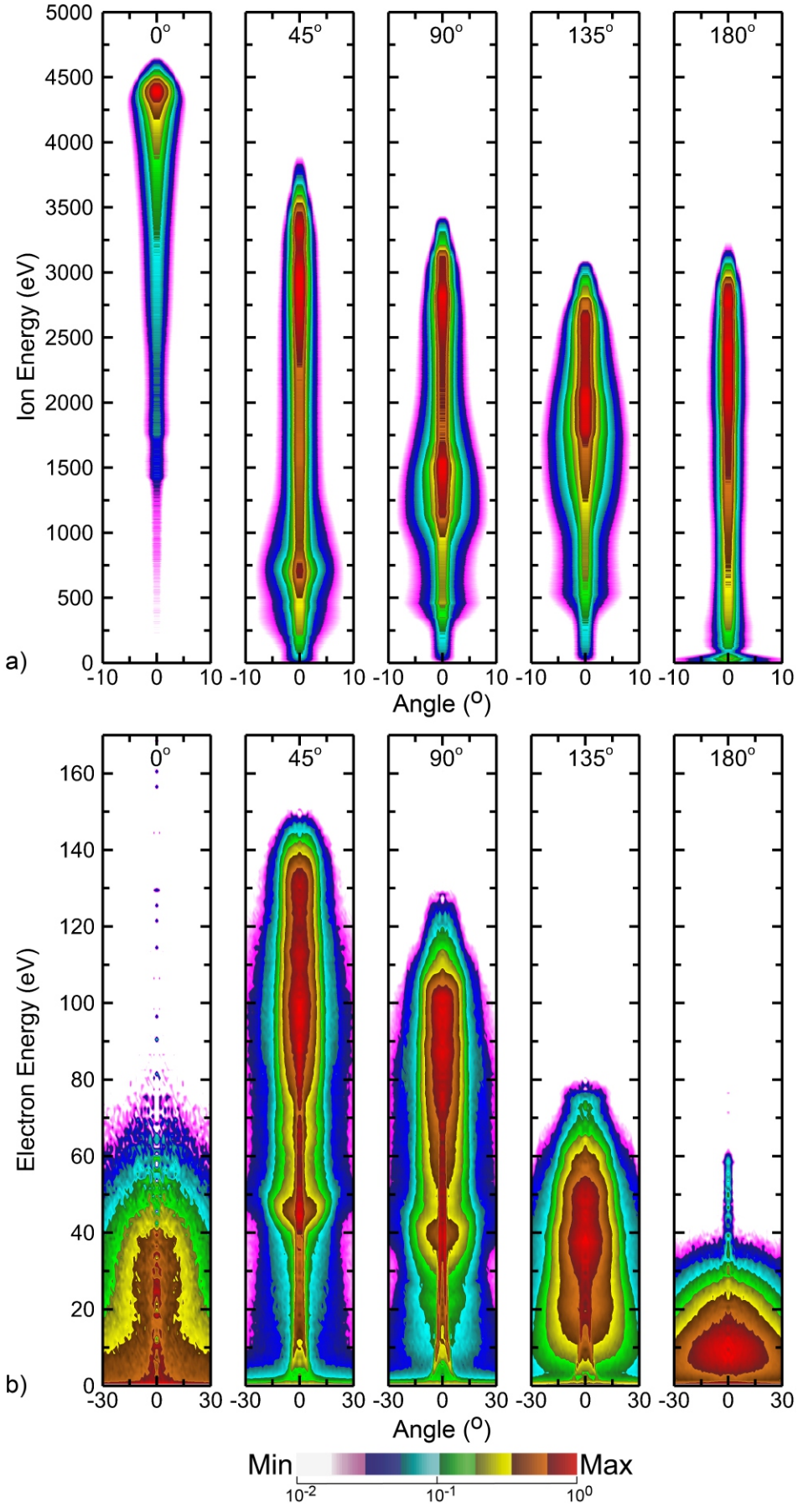

Kruger et al,
Fig. 12 of 14

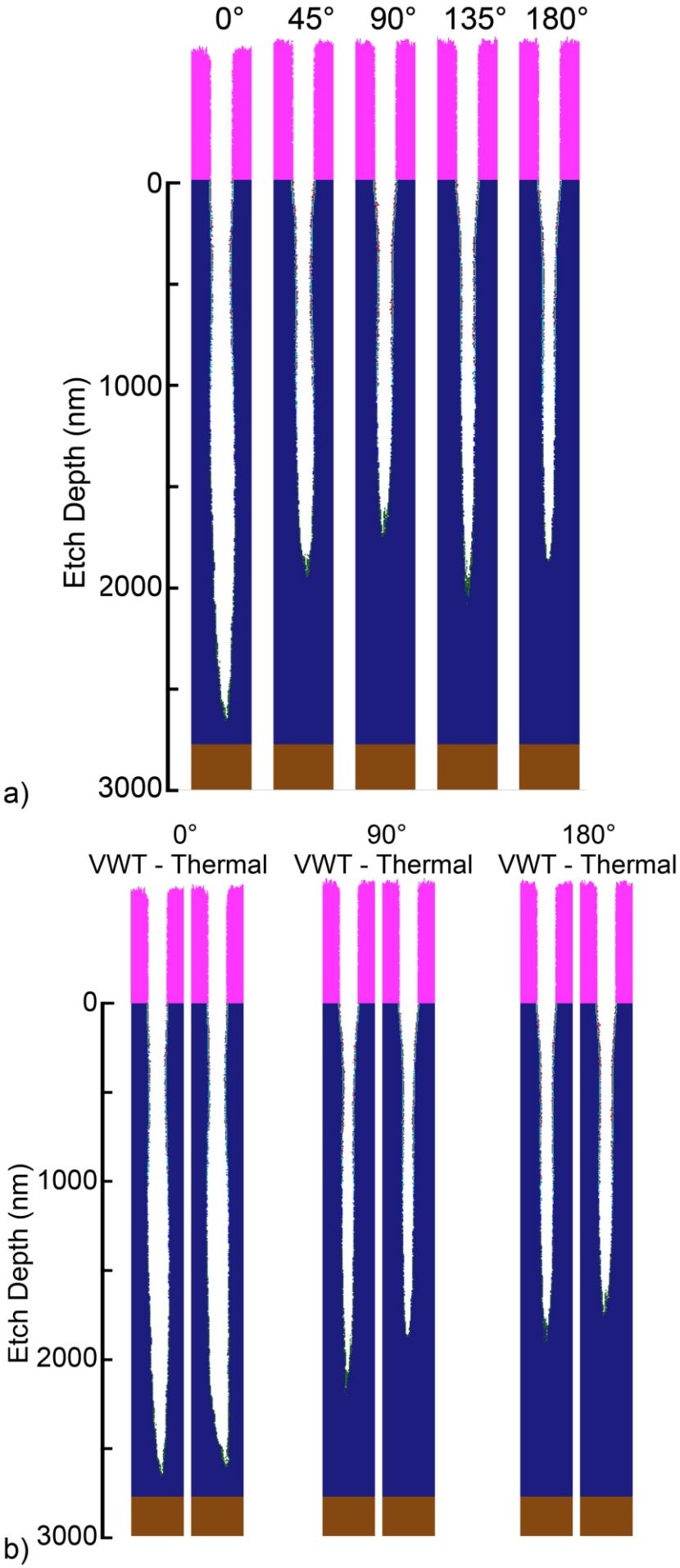

Kruger et al,
Fig. 13 of 14

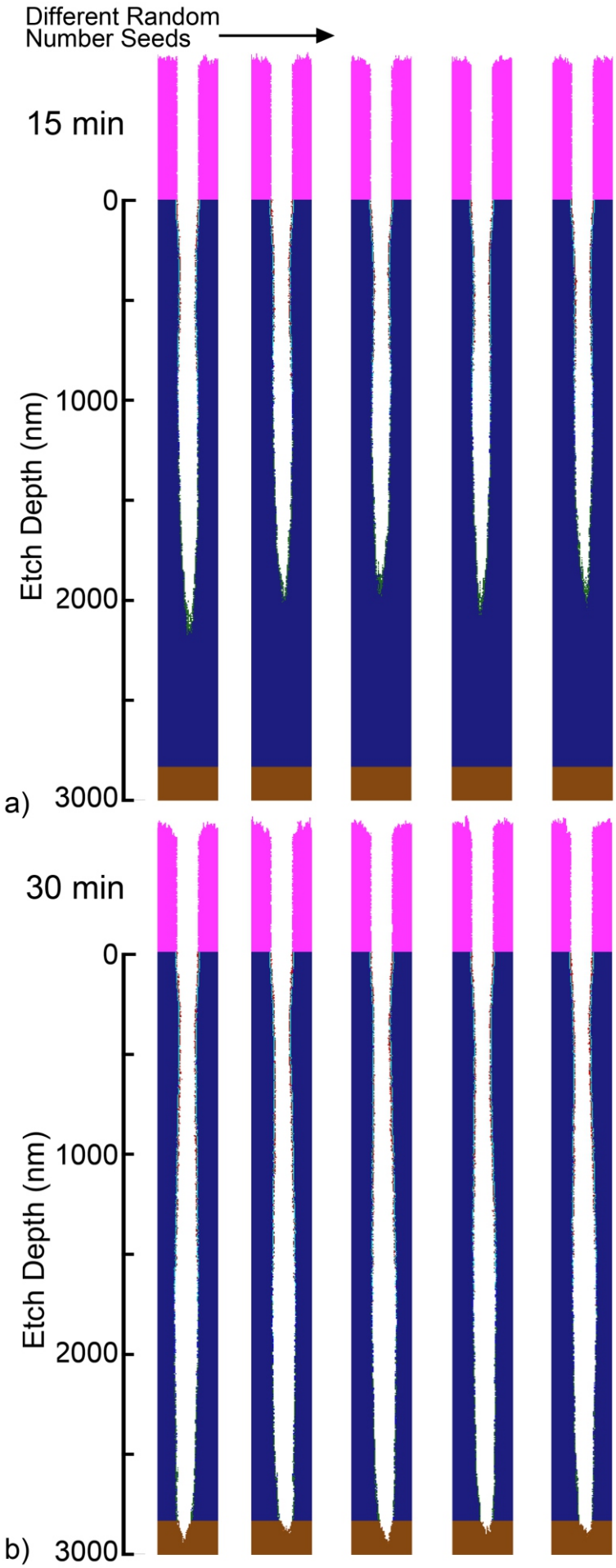

Kruger et al,
Fig. 14 of 14